Numerical study of Dean vortices in developing Newtonian and viscoelastic flows through a curved duct of square cross-section

Mohammed Boutabaa [a], Lionel Helin [b], Gilmar Mompean [b,*], Laurent Thais [b]

[a] *Département de mécanique, faculté des sciences de l'ingénieur, Université de Chlef, Algérie*
[b] *Laboratoire de mécanique de Lille, UMR-CNRS 8107, Polytech-Lille, cité scientifique, 59655 Villeneuve d'Ascq cedex, France*

Abstract

This study is devoted to the three-dimensional numerical simulation of developing secondary flows of Newtonian and viscoelastic fluids through a curved duct of square cross-section. The Phan-Thien–Tanner (PTT) model is used to represent viscoelastic effects. The numerical method uses a finite volume discretization with a staggered grid, and the equations are written in general orthogonal coordinates. The numerical simulations produced for 3 different Dean numbers (125, 137 and 150) show clearly the presence of two steady Dean cells and the upstream development of a four-cell pattern when the centrifugal forces become significant. The comparison between Newtonian and PTT flows shows that the transition from twin-cells to four-cells is anticipated for the viscoelastic fluid. *To cite this article: M. Boutabaa et al., C. R. Mecanique 337 (2009).*
© 2008 Académie des sciences. Published by Elsevier Masson SAS. All rights reserved.

Résumé

Étude numérique des vortex de Dean de fluides Newtonien et viscoélastique en écoulement non établi dans une conduite courbe à section carrée. Cette étude est consacrée à la simulation numérique tridimensionnelle des écoulements secondaires de Dean au sein d'un fluide Newtonien et d'un fluide viscoélastique de Phan-Thien–Tanner s'écoulant dans une conduite courbe de section carrée. La méthode des volumes finis avec un maillage décalé est utilisée pour résoudre les équations de conservation de masse, de quantité de mouvement et l'équation constitutive de PTT écrites en coordonnées orthogonales généralisées. Les calculs faits pour des nombres de Dean de 125, 137 et 150 montrent clairement la présence de deux cellules de Dean et le développement de quatre cellules en aval de la conduite lorsque les forces centrifuges deviennent importantes. Les résultats montrent également que le passage du mode « deux cellules » au mode « quatre cellules » est anticipé pour le fluide viscoélastique. *Pour citer cet article : M. Boutabaa et al., C. R. Mecanique 337 (2009).*
© 2008 Académie des sciences. Published by Elsevier Masson SAS. All rights reserved.

---

* Corresponding author.
 E-mail address: gilmar.mompean@polytech-lille.fr (G. Mompean).

1. Introduction

Dean vortices are the result of centrifugal forces. They are present in a variety of practical applications including technological and physical problems: internal turbine blades, cooling passages, biological systems, ducting in internal combustion engines and heat exchangers.

The first mathematical analysis made by Dean [1] shows the onset of a pair of counter-rotating vortex cells in a Newtonian fluid flow in a curved channel resulting from the interaction between centrifugal and viscous forces. In this paper, Dean introduces a dimensionless number $D_n = R_e \sqrt{a/R_1}$ (subsequently named the Dean number), where R_e is the Reynolds number ($R_e = \rho a U / \mu$, ρ is the fluid density, μ is the dynamic viscosity, a is the channel gap and U is the bulk velocity), and R_1 the inner curvature radius of the channel. The Dean number represents a ratio of the centrifugal forces to the viscous forces, and measures the intensity of the secondary flows. Henceforth, many definitions of the Dean number have been used in the analysis of flows in curved channels and a review is given by Berger et al. [2].

Several works, both theoretical and experimental, have been performed on Dean instabilities, treating the hydrodynamic aspect, thermo-hydrodynamic interactions, and impact on mixture phenomena. For Newtonian fluids, a theoretical analysis performed by Ito [3] shows the existence of secondary flows in a curved channel of rectangular cross section. Targett et al. [4] obtained numerical solutions for the flow in an annulus between two concentric cylinders, of large and infinite aspect ratio, and very small gap. They found a critical Dean number, 37.3, close to the theoretically predicted value by Dean [1]. Cheng and Akiyama [5] used a finite-difference formulation to calculate the secondary flows in curved rectangular ducts. They calculated the familiar two-vortex cell and only mentioned the existence of a new four-vortex cell beyond a critical value of the Dean number. The four-vortex pattern was later presented by Cheng et al. [6]. The numerical investigation by Joseph et al. [7] also showed the switch from the twin counter-rotating vortices to the four-vortex pattern above a critical Dean number. They confirmed the presence of the four-vortex pattern by flow visualization. The appearance of more than one pair of cells was demonstrated for square sections by Soh [8] and Bara et al. [9].

Many researchers extended the study to non-Newtonian fluids, as the analytical study of second order fluids flow in curved pipes made by Jitchote and Robertson [10]. Chen et al. [11] studied viscoelastic flow in rotating curved pipes. Phan-Thien and Zheng [12] present a similarity solution for the Oldroyd-B fluid flow in a narrow curved channel. Joo and Shaqfeh [13] showed the existence of a purely elastic instability in an Oldroyd-B fluid flow. Xue et al. [14] used an implicit finite volume method to investigate numerically the pattern and strength of the secondary flow in rectangular pipes for a general class of viscoelastic model. The present work is focused on exploring Dean vortices in Newtonian and viscoelastic Phan-Thien–Tanner flows in a curved duct of square section, with an average curvature ratio $a/R_c = 0.066$, where R_c is the medium radius of curvature of the channel.

2. Governing equations

The problem is governed by the mass and momentum conservation equations, and the constitutive equation of the Phan-Thien–Tanner viscoelastic fluid which connects the extra-stress components to the velocity field.

2.1. Mass conservation equation

For an incompressible flow:

$$\nabla \cdot \boldsymbol{u} = 0 \tag{1}$$

where $\boldsymbol{u}$ is the velocity vector and ∇ the gradient operator.

2.2. Momentum conservation equation

$$\rho(D\boldsymbol{u}/Dt) = \nabla \cdot (-p\boldsymbol{I} + 2\eta_s \boldsymbol{S} + \boldsymbol{\tau}) \tag{2}$$

where D/Dt is the material derivative, ρ the fluid density, p the Lagrange multiplier arising from incompressibility, $\boldsymbol{I}$ the matrix identity, η_s the solvent viscosity, $\boldsymbol{\tau}$ the polymeric contribution to the extra-stress tensor and $\boldsymbol{S} = 1/2(\nabla \boldsymbol{u} + \nabla \boldsymbol{u}^T)$ the (symmetric) rate-of-deformation tensor.

2.3. Constitutive equation of Phan-Thien–Tanner model

The constitutive equation of the Phan-Thien–Tanner fluid can be expressed in the following general form:

$$f(\{\boldsymbol{\tau}\})\boldsymbol{\tau} + \lambda(D\boldsymbol{\tau}/Dt - \boldsymbol{\tau}\nabla\boldsymbol{u} - \nabla\boldsymbol{u}^t\boldsymbol{\tau}) = 2\eta_p \boldsymbol{S} \tag{3}$$

We used the exponential form presented in Phan-Thien [15] where the function f is defined as

$$f(\{\boldsymbol{\tau}\}) = \exp\big((\varepsilon\lambda/\eta_p)\{\boldsymbol{\tau}\}\big) \tag{4}$$

where η_p represents the polymeric viscosity, $\{\boldsymbol{\tau}\}$ the trace of tensor $\boldsymbol{\tau}$, λ the relaxation time and ε a parameter characterizing the elongational behaviour of the model. For $\varepsilon = 0$, the model reduces to the Oldroyd-B fluid.

2.4. Governing equations in general orthogonal coordinates

The use of general orthogonal coordinates carries out a particular interest to simulate flows in ducts presenting curves or acute borders and flows around bluff bodies. This method was applied by Pope [16] to solve a 2D turbulent recirculating flow in a diffuser. Thais et al. [17] used a similar technique to simulate a laminar unsteady flow past a circular cylinder. By adopting generalized orthogonal coordinates, the problem's equations in tensorial form become (see Pope [16] and Aris [18] for the rules of transformation).

2.4.1. Mass conservation

$$\sum_i \nabla \cdot_{(i)} (V_i) = 0 \tag{5}$$

where V_i represents the physical curvilinear velocity components obtained from normalization of the contravariant velocity components.

2.4.2. Momentum conservation

$$\frac{\partial(\rho V_j)}{\partial t} + \sum_i \nabla \cdot_{(i)} (\rho V_i V_j - T_{ij}) = -\frac{\partial p}{\partial \xi_j} - \sum_i H_j^i(\rho V_i V_j - T_{ij}) + \sum_i H_i^j(\rho V_i V_i - T_{ii}) \tag{6}$$

where $T_{ij} = \tau_{ij} + 2\eta_s S_{ij}$ is the sum of the physical curvilinear components of the polymeric extra-stress tensor τ_{ij} and of the Newtonian stress components and H_i^j represent the stretching factors of the coordinate transform.

2.4.3. Phan-Thien–Tanner constitutive equation

$$f(\{\tau_{ij}\})\tau_{ij} + \lambda\Bigg\{ \frac{\partial \tau_{ij}}{\partial t} + \sum_k \nabla \cdot_{(k)} (V_k \tau_{ij}) - \sum_k H_k^i V_k \tau_{kj} + \sum_k H_i^k V_i \tau_{kj}$$
$$- \sum_k H_k^j V_k \tau_{ik} + \sum_k H_j^k V_j \tau_{ik} - \sum_k L_{ik} \tau_{kj} - \sum_k L_{jk} \tau_{ki} \Bigg\} = 2\eta_p S_{ij} \tag{7}$$

with L_{ij} the components of the generalized velocity gradient operator.

3. Numerical method

3.1. Spatial discretization

The finite volume method is employed to discretize the equations in space with a staggered grid, as proposed by Patankar [19]. The pressure and the normal stress components of the viscoelastic tensor are located at the centre of the control volumes. The velocities are stored and evaluated at the center of the faces of the control volumes. The off-diagonal terms of the viscoelastic tensor are located at the mid-edges of the control volume faces.
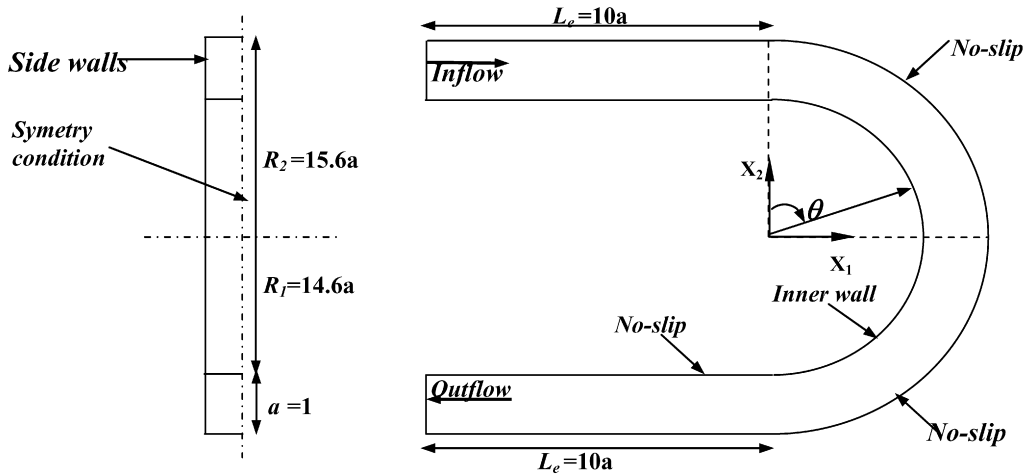
Fig. 1. Geometry of the channel and boundary conditions.

The diffusion terms of the momentum equations are calculated with the second-order accurate centred difference scheme. The non-linear terms (convective fluxes) of the momentum equations and the advection terms of the constitutive equation for the PTT model are evaluated with an upwind quadratic scheme. To improve stability, the EVSS (elastic viscous split stress) algorithm developed by Rajagopalan et al. [20] is used.

3.2. Time discretization

The decoupling procedure used for the pressure is derived from the Marker and Cell algorithm of Harlow and Welch [21]. Details of this procedure are well documented in Mompean and Deville [22]. The symmetric linear system obtained for the pressure is solved by direct Choleski factorization.

3.3. Geometry, mesh and boundary conditions

The channel, as shown in Fig. 1, is divided in three parts: (i) a square straight channel of width $a = 1$ and length $L_e = 10a$ at the entrance; (ii) a connected 180° curved channel with internal radius $R_1 = 14.6a$ and external radius $R_2 = 15.6a$; and (iii) another square straight channel at the exit having the same dimensions as the inlet channel. The origin of the Cartesian coordinates is taken at the center O of the curved channel. A non-uniform spaced mesh has been used: 95 nodes in the streamwise direction (11 nodes located on both straight parts of the channel and the rest uniformly spaced in the curved part), 31 nodes in the normal direction and 16 nodes in the spanwise direction. The analytical solution of a fully developed Newtonian square duct flow is imposed at the inlet and at the outlet of the channel. This solution consists of a rapidly converging power series expansion with a maximum velocity located at the center of the duct 2.096 times the bulk velocity. As mentioned in Fig. 1, the no-slip condition is employed on the walls, and a symmetry condition is employed along the median plane of the duct.

4. Results

In this section we present the evolution of Dean vortices along the curved duct (average curvature ratio $a/R_c = 0.066$) for Newtonian and PTT fluids at Dean numbers $Dn = 125$, 137 and 150. In all figures we show contour lines of the non-dimensional stream function Ψ; to facilitate inter-comparison the extreme values of Ψ are the same on each frame.

4.1. Newtonian flow

At $Dn = 125$, the flow keeps a two-vortex structure until the exit of the curved part of the duct. In Fig. 2 we represent vortex structures at positions $\theta = 40°$, 90° and 180°. For this Dean number, the centrifugal forces are not large enough
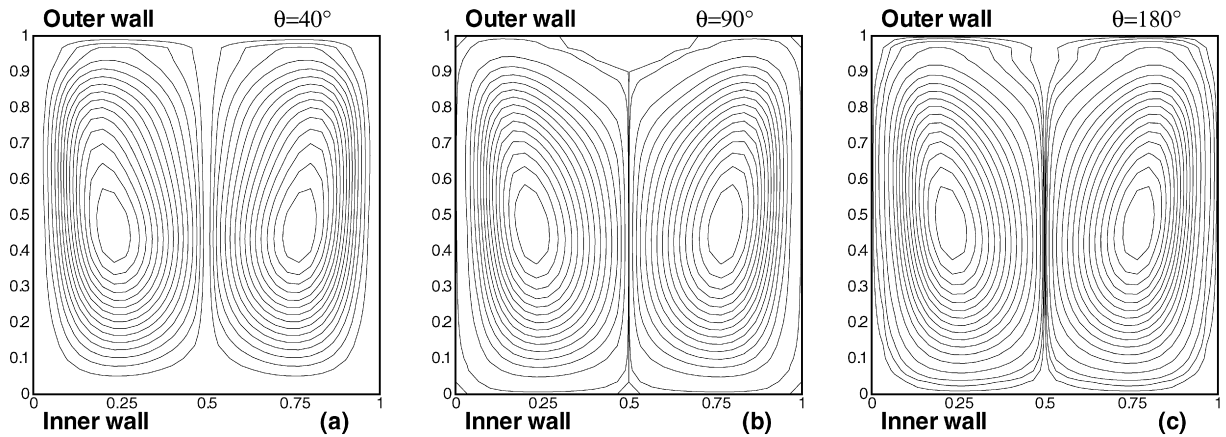
Fig. 2. Stream function at Dean number $Dn = 125$ for Newtonian fluid. (a) $\theta = 40°$, (b) $\theta = 90°$, (c) $\theta = 180°$.
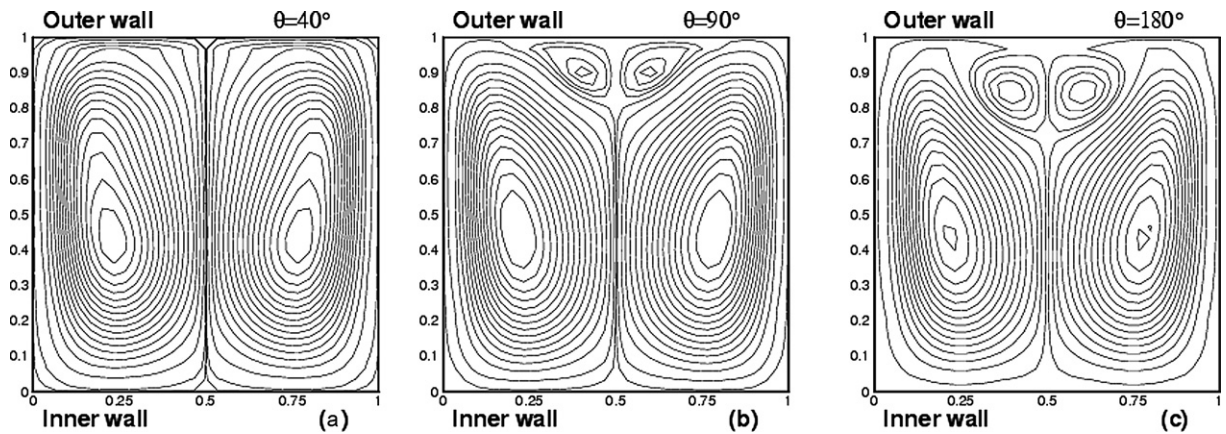

Fig. 3. Stream function at Dean number $Dn = 137$ for Newtonian fluid. (a) $\theta = 90°$, (b) $\theta = 100°$, (c) $\theta = 180°$.

to cause the formation of the additional vortices so the two-vortex flow structure remains intact. However, at $Dn = 137$ (Fig. 3) viscous effects can no longer retain the two-vortex structure, so an additional pair of vortices starts to appear at $\theta = 90°$. This result is in agreement with Bara et al. [9]. At $Dn = 150$ (Fig. 4) the centrifugal forces are even stronger, and the additional pair of vortices starts to form at $\theta = 80°$ (Fig. 4(b)), and is clearly seen at $\theta = 90°$ (Fig. 4(c)). Also the growth rate of the additional vortices is faster than at $Dn = 137$. Bara et al. [9] also observed the appearance of additional vortices at $\theta = 80°$ for $Dn = 150$. Fig. 4(d)–(f) shows the development of the four-cell pattern until the exit of the curved duct.

4.2. Non-Newtonian flow

For the non-Newtonian flow of the PTT fluid, calculations are made for a Deborah number $D_e = \lambda U/a = 0.3$, a viscosity ratio $\eta_s/(\eta_s + \eta_p) = 1/9$ and a material parameter $\varepsilon = 0.1$. In Fig. 5, we plot the vortex structure at $\theta = 40°$, $\theta = 90°$ and $\theta = 180°$ at $Dn = 125$. A similar evolution to the Newtonian case is observed, a two-cell pattern is maintained along the curved duct. As shown in Fig. 6, at $Dn = 137$ the additional vortices appear at $\theta = 80°$ (Fig. 6(b)) earlier than in the Newtonian flow for which the onset was observed at $\theta = 90°$. In Fig. 7 at $Dn = 150$, we show the switch from twin-cells to four-cells (Fig. 7(a)–(b)) and the development of the four-cell pattern until the curved duct exit (Fig. 7(c)–(f)). At this Dean number, the same trend is observed, the additional vortices appear at $\theta = 70°$, earlier than in the Newtonian case for which they appear at $\theta = 80°$. We also remark that the strength and size of the small vortex pair are slightly larger in the non-Newtonian flows.
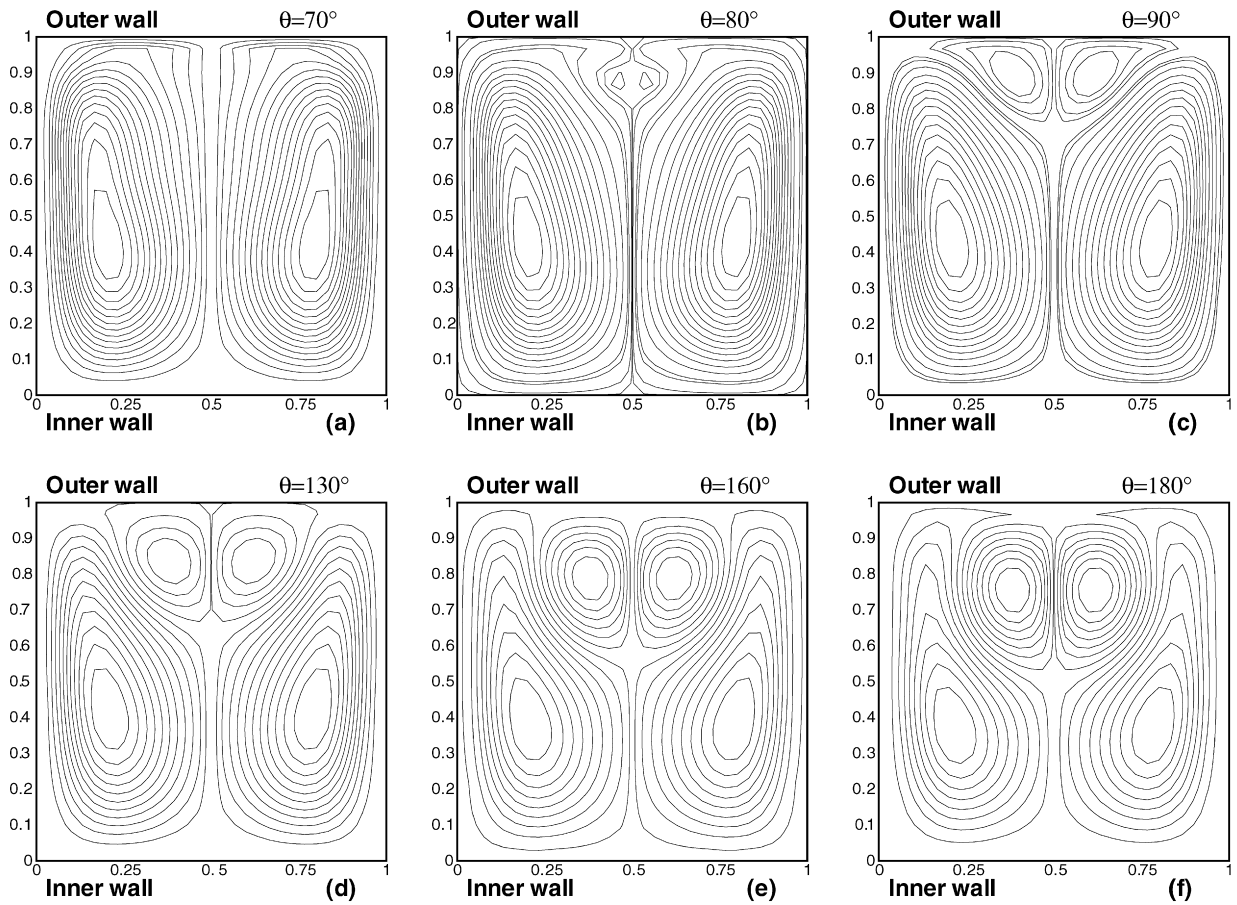
Fig. 4. Stream function at Dean number $Dn = 150$ for Newtonian fluid. (a) $\theta = 70°$, (b) $\theta = 80°$, (c) $\theta = 90°$, (d) $\theta = 130°$, (e) $\theta = 160°$, (f) $\theta = 180°$.
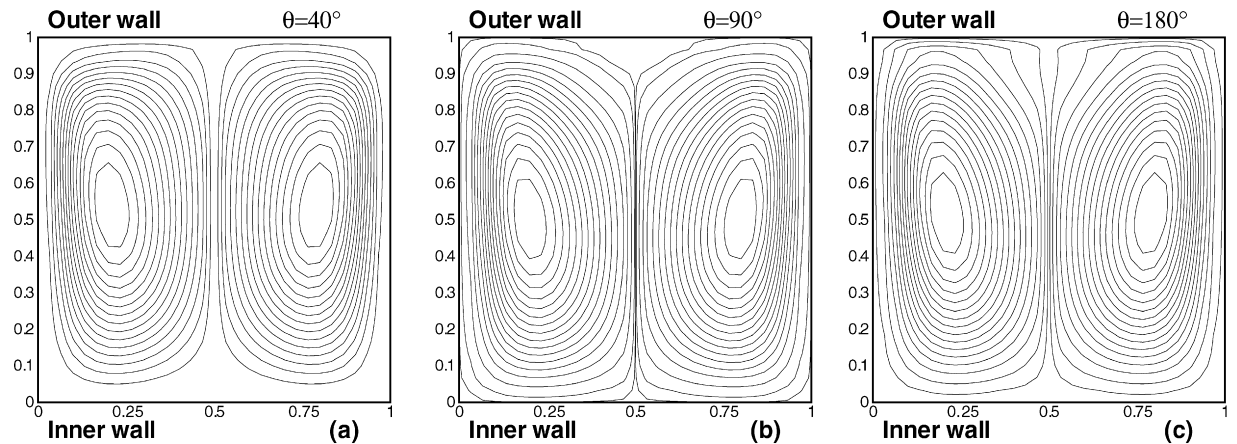

Fig. 5. Stream function at Dean number $Dn = 125$ and Deborah number $D_e = 0.3$ for PTT fluid. (a) $\theta = 40°$, (b) $\theta = 90°$, (c) $\theta = 180°$.

5. Conclusions

This study shows that in both cases, Newtonian and non-Newtonian, the size and the number of Dean vortices depend on the Dean number. The development length (distance from the curved part of the duct to the position of
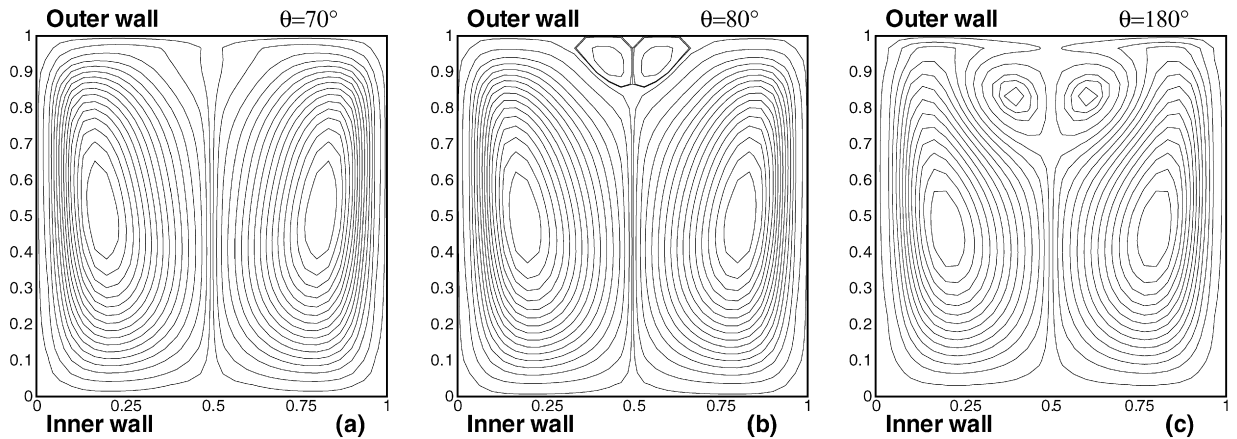
Fig. 6. Stream function at Dean number $Dn = 137$ and Deborah number $D_e = 0.3$ for PTT fluid. (a) $\theta = 70°$, (b) $\theta = 80°$, (c) $\theta = 180°$.
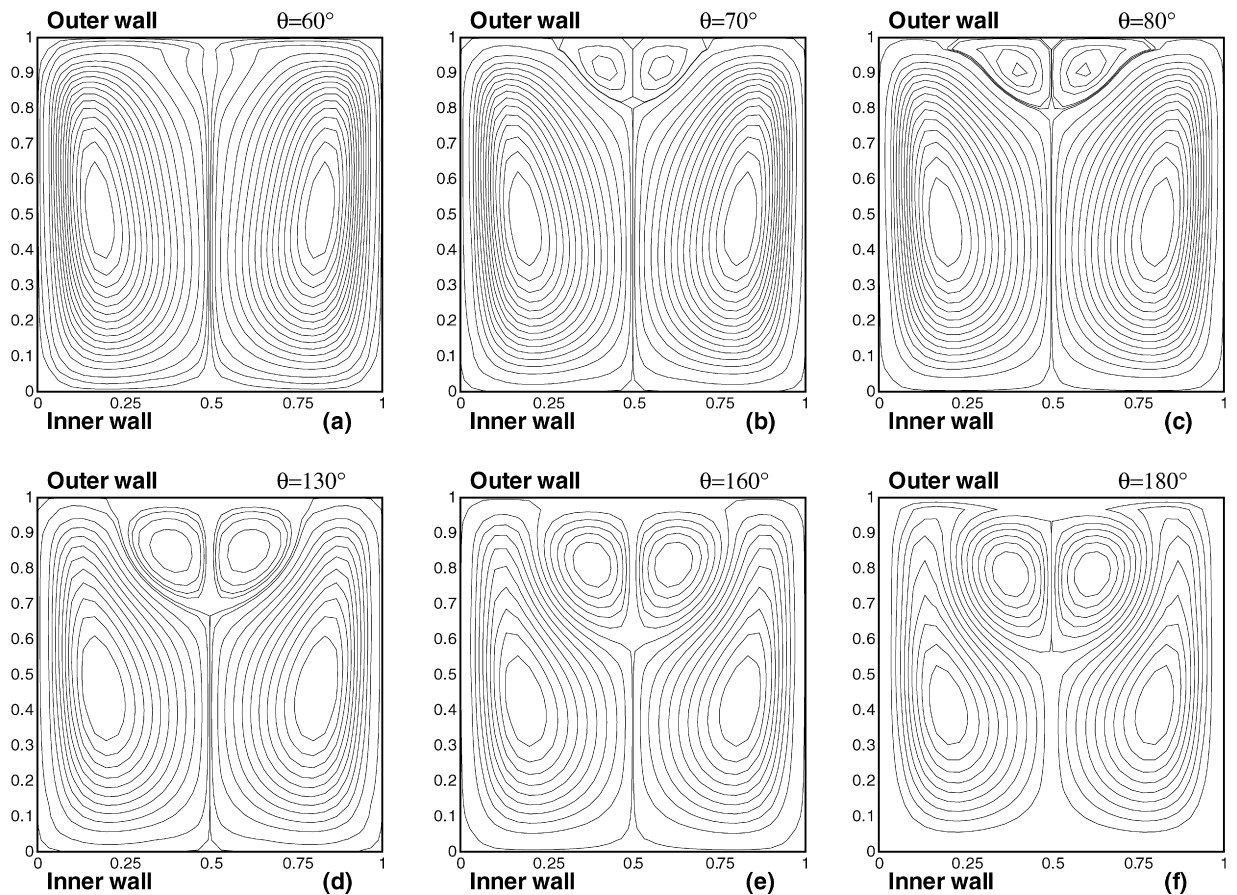

Fig. 7. Stream function at Dean number $Dn = 150$ and Deborah number $D_e = 0.3$ for PTT fluid. (a) $\theta = 60°$, (b) $\theta = 70°$, (c) $\theta = 80°$, (d) $\theta = 130°$, (e) $\theta = 160°$, (f) $\theta = 180°$.

the onset of additional cells) decreases with increasing Dean number. The viscoelasticity affects secondary flows. It is shown clearly that for the PTT fluid, the switch from twin-cells to four-cells appears earlier than in the Newtonian fluid. It is also observed that the growth rate of additional vortices is larger in the non-Newtonian case. This behaviour is similar to the perturbation analysis by Robertson and Muller [23] who also found that viscoelasticity tends to

enhance secondary motions for an Oldroyd-B flow in curved pipes. For future work, it is suggested to undertake a detailed study of the persistence of the secondary flow in the straight outlet section (this would require a longer outlet channel).

References

[1] W.R. Dean, Fluid motion in a curved channel, Proc. R. Soc. London, Ser. A 121 (1928) 402–420.

[2] S.A. Berger, L. Talbot, L.-S. Yao, Flow in curved pipes, Annu. Rev. Fluid Mech. 15 (1983) 461–512.

[3] H. Ito, Theory on laminar flow through curved pipes of elliptic and rectangular cross sections, in: Rep. Inst. High Speed Mech., Tohoku Univ., Sendai, Japan, vol. 1, 1951, pp. 1–16.

[4] M.J. Targett, W.B. Retallick, S.W. Churchill, Flow through curved rectangular channels of large aspect ratio, AIChE J. 41 (1995) 1061–1070.

[5] K.C. Cheng, M. Akiyama, Laminar forced convection heat transfer in curved rectangular channels, Int. J. Heat Mass Transfer 13 (1970) 471–490.

[6] K.C. Cheng, R.-C. Lin, J.-W. Ou, Fully developed laminar flow in curved rectangular channels, Trans. ASME C: J. Fluids Engrg. 98 (1976) 41–48.

[7] B. Joseph, E.P. Smith, R.J. Alder, Numerical treatment of laminar flow in helically coiled tubes of square cross section. Part 1. Stationary helically coiled tubes, AIChE J. 21 (1975) 965–974.

[8] W.Y. Soh, Developing fluid flow in a curved duct of square cross-section and its fully developed dual solutions, J. Fluid Mech. 188 (1988) 337–361.

[9] B. Bara, K. Nandakumar, J.H. Masliyah, An experimental and numerical study of the Dean problem: flow development towards two-dimensional multiple solutions, J. Fluid Mech. 244 (1992) 339–376.

[10] W. Jitchote, A.M. Robertson, Flow of second order fluids in curved pipes, J. Non-Newtonian Fluid Mech. 90 (2000) 91–116.

[11] Y. Chen, H. Chen, J. Zhang, B. Zhang, Viscoelastic flow in rotating curved pipes, Phys. Fluids 18 (2006) 083103.

[12] N. Phan-Thien, R. Zheng, Viscoelastic flow in a curved channel: A similarity solution for the Oldroyd-B fluid, J. Appl. Math. Phys. 41 (1990) 766–781.

[13] Y.L. Joo, E.S.G. Shaqfeh, Viscoelastic Poiseuille flow through a curved channel: A new elastic instability, Phys. Fluids A 3 (9) (1991) 2043–2046.

[14] S.-C. Xue, N. Phan-Thien, R.I. Tanner, Numerical study of secondary flows of viscoelastic fluid in straight pipes by an implicit finite volume method, J. Non-Newtonian Fluid Mech. 59 (1995) 191–213.

[15] N. Phan-Thien, A nonlinear network viscoelastic model, J. Rheol. 22 (1978) 259–283.

[16] S.B. Pope, The calculation of turbulent recirculating flows in general orthogonal coordinates, J. Comp. Phys. 26 (1978) 197–217.

[17] L. Thais, L. Helin, G. Mompean, Numerical simulation of viscoelastic flows with Oldroyd-B constitutive equation and novel algebraic stress models, J. Non-Newtonian Fluid Mech. 140 (2006) 145–158.

[18] R. Aris, Vectors, Tensors and the Basic Equations of Fluid Mechanics, Dover Publications Inc., New York, 1962.

[19] V.S. Patankar, Numerical Heat Transfer and Fluid Flow, Hemisphere Publishing Corporation, New York, 1980.

[20] D. Rajagopalan, R.C. Amstrong, R.A. Brown, Finite element methods for calculation of steady, viscoelastic flow using constitutive equations with a Newtonian viscosity, J. Non-Newtonian Fluid Mech. 36 (1990) 159–192.

[21] F.H. Harlow, J.E. Welch, Numerical calculation of time-dependent viscous incompressible fluid with free surface, Phys. Fluids 8 (1965) 2182–2189.

[22] G. Mompean, M. Deville, Unsteady finite volume simulation of Oldroyd-B through a three-dimensional planar contraction, J. Non-Newtonian Fluid Mech. 72 (1997) 847–859.

[23] A.M. Robertson, S.J. Muller, Flow of Oldroyd-B fluids in curved pipes of circular and annular cross-section, Int. J. Non-Linear Mech. 31 (1996) 1–20.